Regulation of lung endothelial permeability and inflammatory responses by prostaglandin A2: role of EP4 receptor

Tomomi Ohmura[a], Yufeng Tian[a], Nicolene Sarich[a], Yunbo Ke[a], Angelo Meliton[a], Alok S. Shah[a], Katrin Andreasson[b], Konstantin G. Birukov[a,†], and Anna A. Birukova[a,†,*]

[a]Lung Injury Center, Section of Pulmonary and Critical Medicine, Department of Medicine, University of Chicago, Chicago, IL 60637; [b]Department of Neurology and Neurological Sciences, Stanford University School of Medicine, Stanford, CA 94305

ABSTRACT **The role of prostaglandin A2 (PGA2) in modulation of vascular endothelial function is unknown. We investigated effects of PGA2 on pulmonary endothelial cell (EC) permeability and inflammatory activation and identified a receptor mediating these effects. PGA2 enhanced the EC barrier and protected against barrier dysfunction caused by vasoactive peptide thrombin and proinflammatory bacterial wall lipopolysaccharide (LPS). Receptor screening using pharmacological and molecular inhibitory approaches identified EP4 as a novel PGA2 receptor. EP4 mediated barrier-protective effects of PGA2 by activating Rap1/Rac1 GTPase and protein kinase A targets at cell adhesions and cytoskeleton: VE-cadherin, p120-catenin, ZO-1, cortactin, and VASP. PGA2 also suppressed LPS-induced inflammatory signaling by inhibiting the NFκB pathway and expression of EC adhesion molecules ICAM1 and VCAM1. These effects were abolished by pharmacological or molecular inhibition of EP4. In vivo, PGA2 was protective in two distinct models of acute lung injury (ALI): LPS-induced inflammatory injury and two-hit ALI caused by suboptimal mechanical ventilation and injection of thrombin receptor–activating peptide. These protective effects were abolished in mice with endothelial-specific EP4 knockout. The results suggest a novel role for the PGA2–EP4 axis in vascular EC protection that is critical for improvement of pathological states associated with increased vascular leakage and inflammation.**

Monitoring Editor
Kozo Kaibuchi
Nagoya University

Received: Sep 7, 2016
Revised: Mar 27, 2017
Accepted: Apr 13, 2017

INTRODUCTION

The endothelial cell (EC) barrier controls physiological mass transport across the vessel but also regulates tissue inflammatory response to bacterial, chemical, and mechanical insults by allowing proinflammatory cytokines and leukocyte transmigration to the sites of injury. Precise control of endothelial barrier and inflammatory status is especially important to avoid devastating complications of infections, traumatic tissue injury, and other pathological conditions and to prevent development of pulmonary or brain edema. Prostaglandins (PGs) are bioactive lipid mediators elevated during inflammation and generated in vivo by enzymatic peroxidation of arachidonic acid (AA). AA peroxidation by cyclooxygenases COX-1 and COX-2 generates the unstable intermediate prostaglandin PGH2, which then is metabolized by various enzymes to generate a spectrum of PGs, including PGE2, PGI2 (prostacyclin), PGF2α, PGD2, and thromboxane A2. Dehydratation of PGE2 yields the cyclopenthenone PG, prostaglandin A2 (PGA2).

Whereas the biological activities of PGE2, PGF2α, and PGI2 have been investigated, the vascular effects of other prostaglandins, such as PGA2, are virtually unknown. PGE2 mediates its effects in target cells by binding to specific G protein–coupled prostanoid receptors: EP1, EP2, EP3, and EP4; PGI2 acts via the IP receptor, and PGF2 α acts via the FP receptor. All of these receptors are expressed in the endothelium (Alfranca *et al.*, 2006), and EP and IP receptors are

This article was published online ahead of print in MBoC in Press (http://www.molbiolcell.org/cgi/doi/10.1091/mbc.E16-09-0639) on April 20, 2017.

*Address correspondence to: Anna A. Birukova (abirukova@som.umaryland.edu).

†Present address: School of Medicine, University of Maryland, Baltimore, MD 21201.

Abbreviations used: AJ, adherens junction; EC, endothelial cell; MLC, myosin light chain; MYPT1, myosin light chain phosphatase; TER, transendothelial electrical resistance; TJ, tight junction; VE-cadherin, vascular endothelial cadherin.

© 2017 Ohmura *et al.* This article is distributed by The American Society for Cell Biology under license from the author(s). Two months after publication it is available to the public under an Attribution–Noncommercial–Share Alike 3.0 Unported Creative Commons License (http://creativecommons.org/licenses/by-nc-sa/3.0).

"ASCB®," "The American Society for Cell Biology®," and "Molecular Biology of the Cell®" are registered trademarks of The American Society for Cell Biology.

expressed in lung tissues (Breyer *et al.*, 2001). A cell surface receptor mediating PGA2 effects has not been defined.

Basal EC barrier control is mediated by cell junctions containing adherens junction (AJ) and tight junction (TJ) protein complexes linked to the peripheral actin cytoskeleton network (Spindler *et al.*, 2010). Increased assembly of AJ complexes containing vascular endothelial cadherin (VE-cadherin), α,β,γ-catenins, and p120-catenin (Bazzoni and Dejana, 2004) and their interactions with cortical cytoskeleton is precisely regulated by small GTPases Rac, Cdc42, and Rap1 (Spindler *et al.*, 2010). Similar to AJs, TJs are composed of integral membrane proteins: occludin, claudins, junctional adhesion molecule-A (JAM-A), and intracellular proteins, including ZO-1 and cingulin (Miyoshi and Takai, 2005). Although AJs and TJs are separate structural entities, under certain conditions, their components may interact with each other, leading to further enhancement of the cell–cell barrier (Birukova *et al.*, 2011b). These interactions are essential for enhancement of the pulmonary endothelial barrier caused by circulating bioactive molecules.

Better understanding of pathophysiological effects and molecular pathways activated by specific PGs is essential to link basic findings with dysregulation of EC behavior in pathologically relevant conditions and ways of pharmacologically correcting endothelial function. For example, stable prostacyclin analogues beraprost and iloprost, which exhibit pronounced vasodilating and antiremodeling effects on vasculature, are widely used to treat pulmonary hypertension (Howard and Morrell, 2005). Effects of other PGs on vascular inflammation and endothelial barrier dysfunction associated with acute lung injury and other inflammatory conditions are far less explored.

This study investigated effects of PGA2 on human lung vascular endothelial hyperpermeability and inflammation caused by barrier disruptive and inflammatory mediators. PGA2 effects were further tested in animal models of acute lung injury caused by bacterial lipopolysaccharide (LPS) or mechanical ventilation at high tidal volume (HTV) combined with intravenous (i.v.) injection of thrombin receptor–activating peptide (TRAP). We identify a receptor mediating barrier-protective and anti-inflammatory effects of PGA2 in pulmonary endothelium and describe the cellular mechanism of cytoskeletal remodeling induced by PGA2 and contributing to protection of lung endothelial barrier.

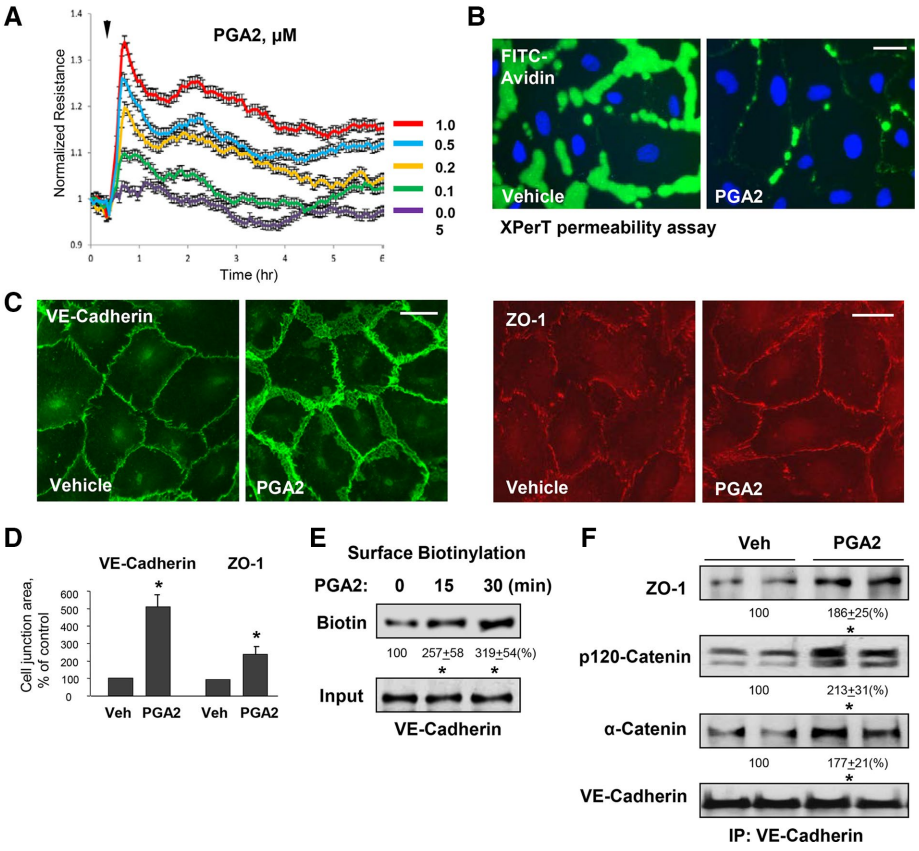

FIGURE 1: PGA2 enhances endothelial barrier and cell junctions. (A) Human pulmonary EC monolayers were grown on gold microelectrodes. At the time point indicated by the arrow, cells were treated with 0.05, 0.1, 0.2, 0.5, or 1 μM PGA2, followed by measurements of TER to reflect EC monolayer barrier properties. (B) Nearly confluent EC monolayers grown on glass coverslips with immobilized biotinylated gelatin were stimulated with vehicle or PGA2 (0.5 μM, 10 min), followed by addition of FITC-avidin (25 μg/ml, 3 min). Unbound FITC-avidin was removed, and FITC fluorescence signal was visualized by fluorescence microscopy; bar, 10 μm. (C) EC monolayers grown on glass coverslips were treated with PGA2 (0.5 μM, 30 min), followed by immunofluorescence staining for VE-cadherin (left) or ZO-1 (right); bar, 10 μm. (D) Quantitative image analysis of VE-cadherin and ZO-1 immunoreactivity at the cell cortical compartment. Results are average ± SD of three independent experiments. (E) ECs were stimulated with PGA2 for indicated periods of time and washed, and cell surface proteins were labeled with Sulfo-NHS-SS-Biotin as described in *Materials and Methods*. Cells were lysed, and biotinylated proteins were precipitated with streptavidin-agarose. Presence of biotinylated VE-cadherin was evaluated by Western blot analysis. Results of densitometry shown as mean ± SD; $n = 4$; $^*p < 0.05$. (F) ECs were treated with PGA2 (0.5 μM, 30 min) or vehicle. After cell lysis, protein complexes were immunoprecipitated with VE-cadherin antibody, followed by Western blot analysis with antibodies to indicated proteins. Equal protein loadings were confirmed by reprobing of membranes with VE-cadherin antibody. Results of densitometry normalized to VE-cadherin are shown as mean ± SD; $n = 4$; $^*p < 0.05$.

RESULTS

Effects of PGA2 on human pulmonary EC barrier and intracellular signaling

Dose-dependent effects of PGA2 on EC barrier properties were monitored by changes in transendothelial electrical resistance (TER) of cell monolayers grown on microelectrodes. PGA2 caused dose-dependent TER increases in the concentration range of 0.05–1 μM (Figure 1A). A barrier-enhancing effect was observed by 2 min of PGA2 stimulation, reached maximal levels by 15–30 min of stimulation, and was sustained in the next 4–6 h after stimulation.

Treatment of preconfluent EC monolayers with PGA2 caused rapid formation of cell–cell contacts and establishment of the EC monolayer, leading to decreased paracellular permeability for macromolecules, as detected by decreased accumulation of fluorescein isothiocyanate (FITC)–labeled avidin on the coating substrate underneath the cells (Figure 1B). In agreement with barrier-enhancing effects on human pulmonary EC monolayers, we saw increased VE-cadherin– and ZO-1–positive areas at the cell–cell junctions of PGA2-treated cells, indicating enhanced AJs and TJs, respectively (Figure 1, C and D).

The PGA2-induced increase in VE-cadherin–positive areas at the cell–cell junctions was further verified by the surface protein biotinylation assay described in *Materials and Methods*. After in situ biotinylation of cell surface proteins in control and PGA2-stimulated cells, the level of biotinylated VE-cadherin was assessed by Western blotting. VE-cadherin surface expression, as reflected by the levels of biotinylated VE-cadherin, increased in PGA2-treated EC monolayers (Figure 1E). These findings are consistent with PGA2-induced EC morphological changes and monolayer barrier function. Coimmunoprecipitation assays with VE-cadherin antibody showed that PGA2-induced enhancement of the EC barrier was also associated with increased association of VE-cadherin with other AJ proteins: p120-catenin, α-catenin, and TJ-associated protein ZO-1 (Figure 1F).

The PGA2-mediated TER increase was accompanied by a rapid increase in intracellular cAMP levels within 2 min (Figure 2A). Direct measurements of small GTPase activation showed that barrier enhancement in response to PGA2 was associated with rapid activation of Rap1 and Rac1 GTPases (Figure 2B), whereas RhoA activity was not affected (unpublished data). As a reflection of elevated cAMP-dependent protein kinase (PKA) enzymatic activity, PGA2 treatment increased phosphorylated levels of PKA substrates cAMP response element binding protein (CREB) and the actin-binding protein vasodilator-stimulated phosphoprotein (VASP; Figure 2C). Tyrosine phosphorylation of a regulator of cortical actin polymerization, cortactin, is promoted by activated Rac1 (Head *et al*., 2003).

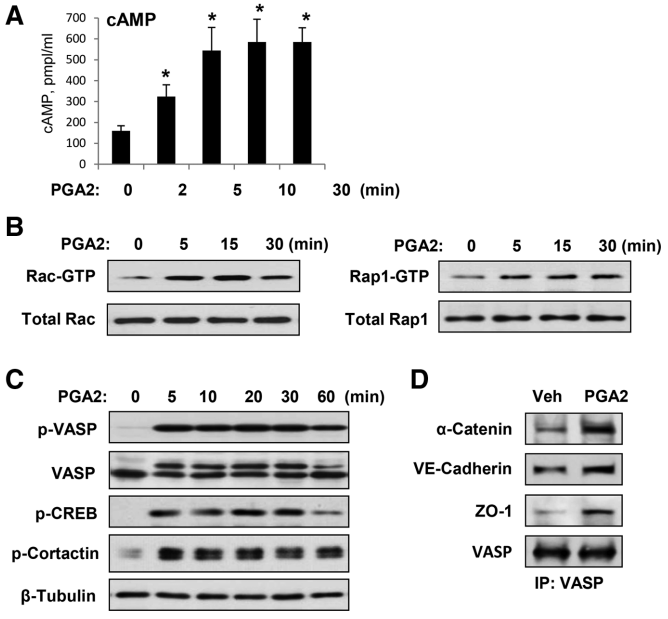

FIGURE 2: Effect of PGA2 on intracellular cAMP level, activation of Rac, and Rap cytoskeletal and cell junction targets. (A) ECs were stimulated with PGA2 (0.5 μM) for indicated periods of time, and intracellular cAMP levels were determined, as described in *Materials and Methods*. Results are mean ± SD of three independent experiments. *$p < 0.001$. (B) PGA2-induced activation of Rac (left) and Rap (right) evaluated using GTPase pull-down assays. Total GTPase content in cell lysates was used as a normalization control. (C) Time-dependent phosphorylation of VASP, CREB, and cortactin determined in the total lysates using phosphoprotein-specific antibodies. (D) Coimmunoprecipitation assay of control and PGA2-stimulated (30 min) ECs using VASP antibody. Coprecipitated proteins were determined by Western blot analysis with appropriate antibody.

Consistent with activation of Rac1, PGA2 caused rapid phosphorylation of cortactin (Figure 2C).

Of interest, coimmunoprecipitation studies showed that PGA2 also stimulated association of VE-cadherin, α-catenin, and ZO-1 with the PKA cytoskeletal target VASP (Figure 2D). These results demonstrate a convergence of PKA- and Rac-mediated signaling pathways on cytoskeletal and cell junction proteins involved in PGA2-induced EC barrier response. Elevation of cAMP by other prostaglandins—PGI2 and PGE2—is mediated by IP and EP receptors (Breyer *et al*., 2001). Therefore we hypothesized that the observed effects of PGA2 on intracellular signaling are mediated by one or more prostaglandin receptors. We tested such receptors in the following experiments.

Screening for potential receptors mediating PGA2 barrier-enhancing response

We screened potential receptors mediating PGA2-induced EC barrier enhancement using specific agonists and inhibitors of prostanoid receptors. EC permeability assays of PGA2-stimulated EC monolayers using TER measurements showed that specific inhibitors of FP, TP, DP2, and IP prostanoid receptors did not affect PGA2-induced EC barrier enhancement response (Figure 3A). EC pretreatment with AH6809, an EP1-3 and DP receptor antagonist with nearly equal affinity for the cloned human EP1, EP2, EP3, and DP1 receptors, also did not affect the barrier-enhancing response to PGA2. In turn, pretreatment with EP4 receptor inhibitor L161982 or GW627368X abolished PGA2-induced EC barrier enhancement (Figure 3, A and B). In turn, stimulation of pulmonary EC with pharmacological EP4 receptor activator CAY10580 recapitulated EC barrier enhancement caused by PGA2 (Figure 3A, right). As an alternative to pharmacological inhibition, we performed molecular inhibition of EP4 receptor by small interfering RNA (siRNA)–induced EP4 knockdown. Treatment with EP4-specific siRNA suppressed the barrier-enhancing effect of PGA2 (Figure 3B).

Activation of G_s-coupled EP4 receptor leads to G_s-dependent activation of adenylate cyclase and elevation of intracellular cAMP levels (Yagami *et al*., 2016). Control experiments (Figure 3C) showed that the EC barrier enhancement response to elevation of intracellular cAMP caused by cell treatment with stable cAMP analogue Br-cAMP or adenylate cyclase activator forskolin was not affected by cell pretreatment with EP4 antagonist. EP4 antagonist did not affect EC barrier enhancement caused by prostacyclin, known to act via the IP receptor, but abolished EC barrier response to PGA2. In turn, IP antagonist was without effect on prostacyclin-induced cell response but inhibited EC barrier enhancement response to PGA2. Taken together, these results show a specific role of EP4 receptor in mediating the pulmonary EC barrier-enhancing response to PGA2.

Effects of EP4 inhibition on PGA2-induced activation of intracellular signaling and cytoskeletal remodeling

Involvement of EP4 in PGA2-induced cytoskeletal remodeling linked to EC barrier enhancement was evaluated using siRNA-induced EP4 knockdown and pharmacological EP4 receptor antagonist L161982. EP4 antagonist abolished PGA2-induced activation of Rac1 and Rap1 (Figure 4A). Analysis of downstream cytoskeletal targets of Rap1/Rac1 and cAMP/PKA signaling showed that inhibition of EP4 by L161982 (Figure 4B) or siRNA-induced EP4 knockdown (Figure 4C) suppressed PGA2-induced phosphorylation of Rac1-dependent regulator of actin polymerization, cortactin and cAMP/PKA substrates, actin-binding protein VASP, and transcription factor CREB.

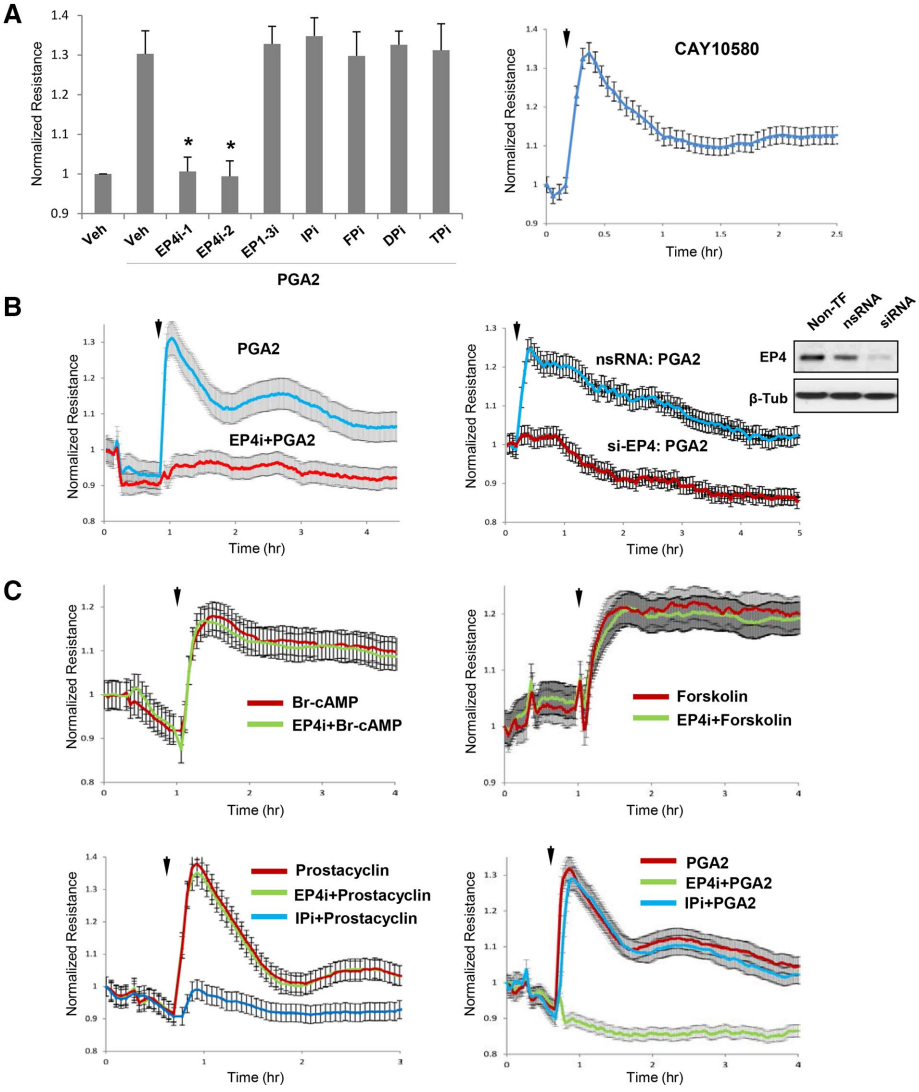

FIGURE 3: Identification of prostaglandin receptor mediating the barrier-enhancing effects of PGA2. (A) ECs were pretreated with antagonists of EP1-3 (AH6809, 25 μM), EP4 (L161982 [EP4i-1], 3 μM; or GW627368X [EP4i-2], 3 μM), IP (CAY10449, 50 nM), FP (AL8810, 3 μM), DP (BWA868C, 50 nM), and TP (SQ29548, 0.5 μM) receptors and stimulated with PGA2 (0.5 μM). Results of TER measurements shown as mean ± SD of three independent experiments; *$p < 0.001$. Right, TER elevation in response to addition of EP4 receptor activator (K10580, 0.2 μM) marked by arrow. (B) Time-dependent analysis of TER changes performed in PGA2-stimulated EC (arrow) pretreated with EP4 inhibitor (left) or EP4-specific siRNA (right). Inset, Western blot verification of siRNA-induced EP4 protein knockdown. (C) Effects of EP4 (L161982) and IP receptor inhibitors on barrier-enhancing effects of Br-cAMP (200 μM), forskolin (1 μM), prostacyclin (0.5 μM), and PGA2 (0.5 μM). Normalized average resistance values from three independent readings in one experiment; the data are representative of three independent experiments.

A role of EP4 in PGA2-activated EC cytoskeletal dynamics critical for EC barrier-enhancing response was further evaluated using live-cell microscopy. Pulmonary ECs expressing green fluorescent protein (GFP)–labeled cortactin were treated with nonspecific or EP4-specific siRNA, followed by stimulation with PGA2. PGA2 stimulated formation of lamellipodia (shown by arrows in Figure 4D, top), also associated with accumulation of GFP-cortactin at the cell periphery. These changes reflect PGA2-induced activation of peripheral cytoskeletal remodeling. This cytoskeletal response was abolished in cells with EP4 knockdown (Figure 4D, bottom). The higher-magnification insets in Figure 4D show details of the peripheral cortactin arrangement. The bar graph depicts a quantitative image analysis of peripheral cortactin accumulation in stimulated control and EP4 knockdown cells.

Next we studied effects of EP4 inhibition on PGA2-induced enhancement of AJs. PGA2 stimulated enlargement of VE-cadherin–positive and ZO-1–positive areas at the cell junctions in EC monolayers, which was abolished by siRNA-induced EP4 knockdown (Figure 5A). In biochemical studies, in situ biotinylation assay showed decreased levels of biotinylated VE-cadherin in PGA2-stimulated ECs pretreated with EP4 antagonist (Figure 5B).

AJ enhancement is associated with increased interactions of AJ proteins. We visualized intracellular colocalization and protein interaction of VE-cadherin and p120-catenin using a proximal ligation assay (PLA). Increased accumulation of both proteins at the cell junction areas of PGA2-stimulated ECs and their interaction was suppressed by EC pretreatment with EP4 receptor inhibitor (Figure 5C).

Coimmunoprecipitation assays with anti-VE-cadherin and anti-VASP antibodies showed that PGA2 increased association of ZO-1, α-catenin, VASP, and VE-cadherin, which was abolished by pretreatment with EP4 receptor inhibitor (Figure 5D). These findings suggest an EP4-dependent mechanism of PGA2-induced enhancement of endothelial AJs and activation of AJ–TJ functional interactions.

PGA2 enhances barrier properties of lung epithelial cells

Epithelial barrier protects the lung from invasion of bacterial particles. In cooperation with pulmonary vascular endothelium, lung epithelial cells form a second barrier to control fluid balance and prevent alveolar flooding and pulmonary edema. We tested effects of PGA2 on barrier properties of small airway epithelial cell (SAES) monolayers using TER measurements. Similar to the response developed by pulmonary ECs, PGA2 caused rapid elevation of TER in SAES in the concentration range of 0.2–3.0 μM (Figure 6A). The barrier-enhancing effect developed within 2–5 min of PGA2 stimulation, reached maximal levels by 15–30 min, and then gradually declined, reaching basal levels by 5 h poststimulation.

SAEC stimulation with PGA2 (0.5 μM) caused time-dependent phosphorylation of regulators of peripheral actin remodeling, VASP and cortactin (Figure 6B, left). Inhibition of EP4 by L161982 suppressed the PGA2-induced phosphorylation of cortactin and VASP (Figure 6B, right). The barrier-enhancing effect of PGA2 and increased phosphorylation of cortactin and VASP were associated with increased F-actin immunoreactivity at the cell periphery (Figure 6C)

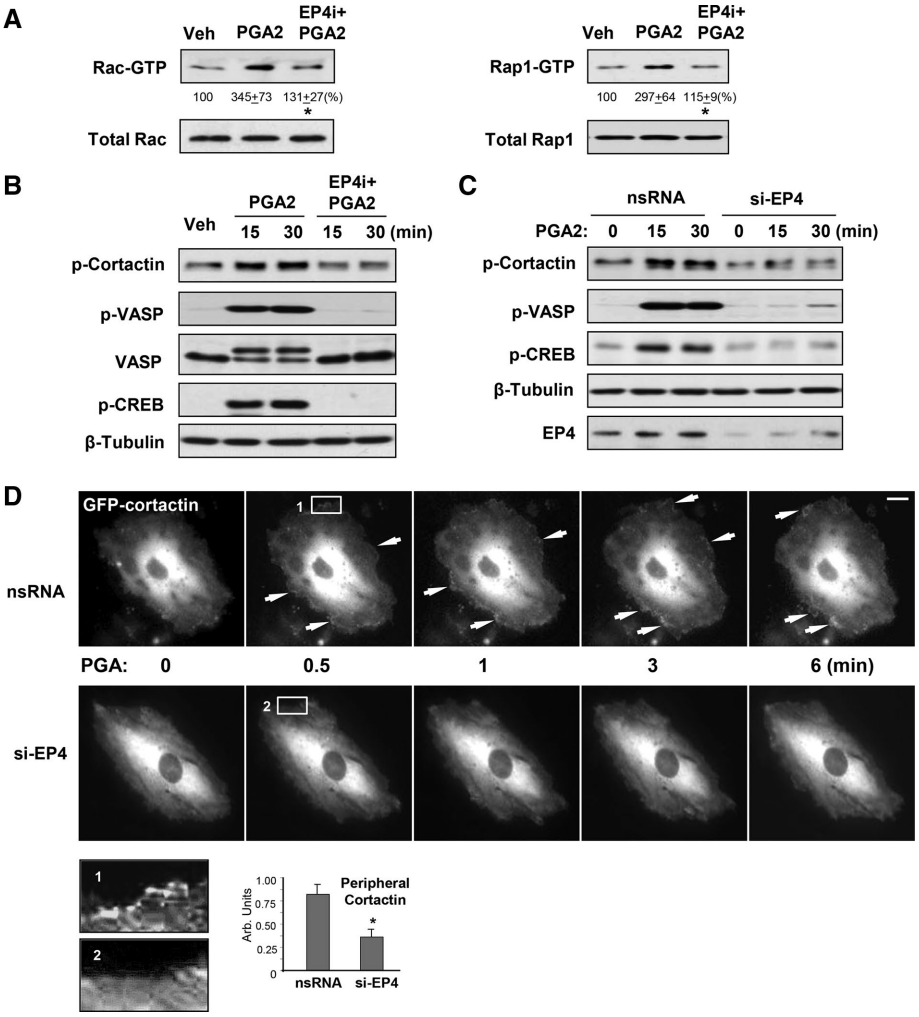

FIGURE 4: Inhibition of EP4 abolishes PGA2-induced activation of Rac and Rap pathways and cytoskeletal remodeling. (A) Pretreatment with EP4 inhibitor abolished PGA2-induced Rac and Rap GTPase activation measured in pull-down assays. Results of densitometry are shown as mean ± SD; $n = 3$; *$p < 0.05$. (B) Pretreatment with EP4 inhibitor L161982 or (C) siRNA-induced EP4 knockdown abolished phosphorylation of PKA and Rac target proteins, as shown by Western blot analysis with phosphospecific antibodies. EP4 knockdown was verified by Western blot with EP4 antibody. Reprobing with β-tubulin antibody was used as a normalization control. (D) Live-cell imaging of EC transfected with EP4 siRNA or nonspecific RNA and expressing GFP-cortactin. Snapshots depict PGA2-induced cortical dynamics (arrows) at the cell periphery of control and EP4-depleted cells. Bar, 5 μm. Higher-magnification insets depict details of peripheral cortactin arrangement. Bar graph gives the results of quantitative image analysis of cortactin accumulation in PGA2-stimulated control and EP4-depleted ECs, shown as mean ± SD; $n = 3$; *$p < 0.05$.

and enhancement of AJs indicated by increased peripheral accumulation of p120-catenin, an AJ adaptor and signaling protein (Figure 6D). These cytoskeletal effects caused by PGA2 were inhibited by cell pretreatment with EP4 inhibitor L161982. The higher-magnification insets depict details of cortical actin remodeling.

EP4 mediates PGA2-induced EC barrier protection against thrombin-induced permeability

To study the physiological role of PGA2 in modulation of agonist-induced EC responses, we evaluated the effect of PGA2 on the endothelial barrier using a model of thrombin-induced EC permeability. Pretreatment of pulmonary EC monolayers with PGA2 suppressed the acute TER decline in response to thrombin (Figure 7A). In addition to TER measurements, we examined PGA2 protective effects against thrombin-induced EC hyperpermeability using an imaging assay detecting EC monolayer permeability for macromolecules (Dubrovskyi *et al.*, 2013). Consistent with TER results, PGA2 attenuated thrombin-induced EC monolayer permeability for FITC-labeled tracer (Figure 7B, left). The barrier-protective effect of PGA2 was abolished by EC pretreatment with EP4 inhibitor (Figure 7B, right). We made similar observations in experiments with EP4 knockdown. We evaluated EC monolayer integrity by immunofluorescence staining for F-actin. Whereas PGA2 suppressed stress fibers and gap formation induced by thrombin, EP4 knockdown abolished PGA2-protective effects (Figure 7C).

Because thrombin-induced disruption of ECl junctions and EC barrier dysfunction are associated with activation of the Rho pathway (Fukata and Kaibuchi, 2001), we next examined effects of PGA2 on the thrombin-induced Rho signaling. Pretreatment with PGA2 markedly suppressed thrombin-induced Rho activation (Figure 7D) and Rho-dependent phosphorylation of myosin light chain phosphatase (MYPT) and myosin light chain (MLC; Figure 7E). In turn, EP4 inhibitor abolished PGA2-mediated inhibition of Rho activation and phosphorylation of MYPT and MLC caused by thrombin (Figure 7, D and E).

EP4 mediates PGA2-induced EC protection against LPS-induced barrier dysfunction and EC inflammatory activation

Bacterial compounds such as LPS cause pronounced activation of inflammatory signaling in pulmonary ECs and disruption of EC monolayers (Fu *et al.*, 2009; Schlegel *et al.*, 2009). We tested the effects of PGA2 on EC barrier dysfunction caused by LPS. LPS decreased TER, reflecting endothelial barrier dysfunction, and PGA2 pretreatment abolished this effect (Figure 8A). Of importance, the protective effect of PGA2 was inhibited by EP4 antagonist.

Activation of the NFκB signaling cascade manifested by phosphorylation of the NFκB subunit and degradation of the inhibitory IκBα subunit is a hallmark of LPS-induced inflammation (Lu *et al.*, 2008; Khakpour *et al.*, 2015). LPS triggered the canonical inflammatory pathway and induced phosphorylation of NFκB and degradation of IκBα. LPS-induced NFκB phosphorylation was suppressed by PGA2, and this anti-inflammatory effect of PGA2 was abolished by cell pretreatment with EP4 inhibitor (Figure 8B). Because our studies showed activation of Rap1/Rac1 and PKA signaling by PGA2 (Figure 2), we tested involvement of these pathways in the PGA2-induced inhibition of NFκB phosphorylation. Inhibition of either PKA or Rac1 activity attenuated PGA2-induced NFκB phosphorylation (Figure 8C), suggesting critical involvement of both PKA and Rac1 signaling in PGA2 anti-inflammatory effects.

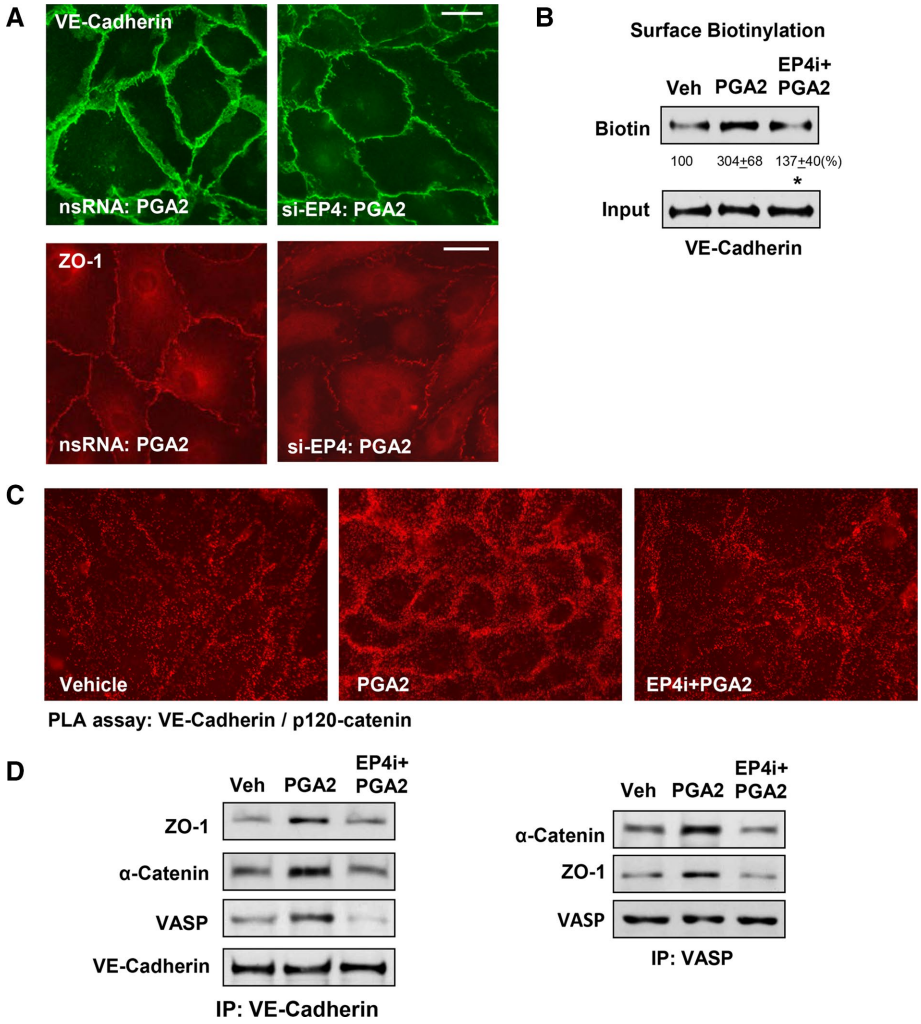

FIGURE 5: Inhibition of EP4 abolishes PGA2-induced enhancement of AJs and TJs. Pretreatment with EP4 inhibitor (L161982, 3 μM). (A) EC transfection with si-EP4 suppressed enlargement of VE-cadherin–positive AJs (left) and enhancement of ZO-1–positive TJs (right; bar, 10 μm) and (B) attenuated increase of surface-biotinylated VE-cadherin in ECs treated with PGA2 (0.5 μM, 30 min). Results of densitometry are shown as mean ± SD; $n = 4$; $^*p < 0.05$. (C) PLA (red) with PGA2-stimulated ECs with or without pretreatment with EP4 inhibitor, using mouse monoclonal anti–p120-catenin and rabbit polyclonal anti–VE-cadherin antibodies. PGA2-increased PLA signals at the area of adherens junctions were suppressed in ECs pretreated with EP4 inhibitor. Bar, 10 μm. (D) Pretreatment with EP4 inhibitor abolished PGA2-induced association of ZO-1, α-catenin, VASP, and VE-cadherin. Protein complexes were immunoprecipitated with VE-cadherin (left) or VASP (right) antibody, followed by Western blot analysis with antibodies to indicated proteins. Equal protein loadings were confirmed by membrane reprobing with VE-cadherin and VASP antibody, respectively. Results are representative of three independent experiments.

Activation of NFκB-dependent inflammatory signaling stimulates expression of ICAM1 and VCAM1, the EC adhesion molecules involved in neutrophil adhesion (Smith, 1993). Pretreatment with PGA2 inhibited LPS-induced expression of ICAM1 and VCAM1, and this protective effect was inhibited by EP4 antagonist (Figure 8D). Similarly, siRNA-induced knockdown of EP4 abolished the protective effect of PGA2 against LPS-stimulated ICAM1 expression (Figure 8E). In accordance with the anti-inflammatory effects of PGA2 on LPS-challenged EC, PGA2 pretreatment also attenuated LPS-induced production of tumor necrosis factor-α (TNFα) and interleukin-6 (IL-6) by pulmonary ECs (Figure 8, F and G, left). Of note, PGA2 was also protective against endothelial barrier disruption induced by EC exposure to individual cytokines (Figure 8, F and G, right).

Effects of PGA2 posttreatment on LPS-induced EC barrier dysfunction

Because treatment of ongoing inflammation with protective compounds represents a more clinically relevant scenario of pharmacological intervention, we next tested the effects of PGA2 against LPS-induced EC barrier dysfunction as a posttreatment option. PGA2 added after 30 min, 2 h, or 5 h of LPS stimulation also had a potent barrier-protective effect, reflected by pronounced and sustained elevation of TER (Figure 9A). This effect was abolished in ECs with siRNA-induced EP4 knockdown (Figure 9B).

Protective effects of PGA2 posttreatment on LPS-induced disruption of EC monolayers were further monitored by analysis of actin cytoskeletal remodeling. Pulmonary ECs were treated with LPS with or without PGA2 added 5 h after LPS challenge. Immunofluorescence staining of actin cytoskeleton was performed 1 h after PGA2 addition. LPS induced formation of paracellular gaps. These changes were reduced by EC posttreatment with PGA2 (Figure 9C, top). Restoration of EC monolayer integrity, gap closure, and disappearance of actin stress fibers caused by PGA2 posttreatment were abolished in EC with EP4 knockdown (Figure 9C, bottom).

Protective effects of PGA2 in animal models of acute lung injury

Protective effects of PGA2 were next tested in the murine models of acute lung injury (ALI). In the model of nonbacterial lung injury, mice were exposed to mechanical ventilation as described in *Materials and Methods* and i.v. injection of TRAP. PGA2 treatment was performed by i.v. administration of PGA2 at the beginning and 2 h later during mechanical ventilation. Injection of sterile phosphate-buffered saline (PBS) was used as a control. After 4 h of mechanical ventilation mice, developed a prominent acute inflammatory response characterized by increased cell counts and protein content in bronchoalveolar lavage (BAL) samples (Figure 10A). These effects were significantly attenuated by injection of PGA2. There was no significant difference in BAL cell count and BAL protein between PGA2-treated animals and a control group without PGA2 treatment in the absence of HTV (unpublished data).

Effects of PGA2 on the lung vascular leak induced by TRAP/HTV were evaluated by measurement of Evans blue extravasation into the lung tissue, as described in *Materials and Methods*. Increased Evans blue accumulation in the lung parenchyma caused by TRAP/HTV was attenuated by PGA2 (Figure 10B). Barrier-protective and anti-inflammatory effects of PGA2 were further tested in the animal model of ALI caused by intratracheal (i.t.) injection of bacterial wall

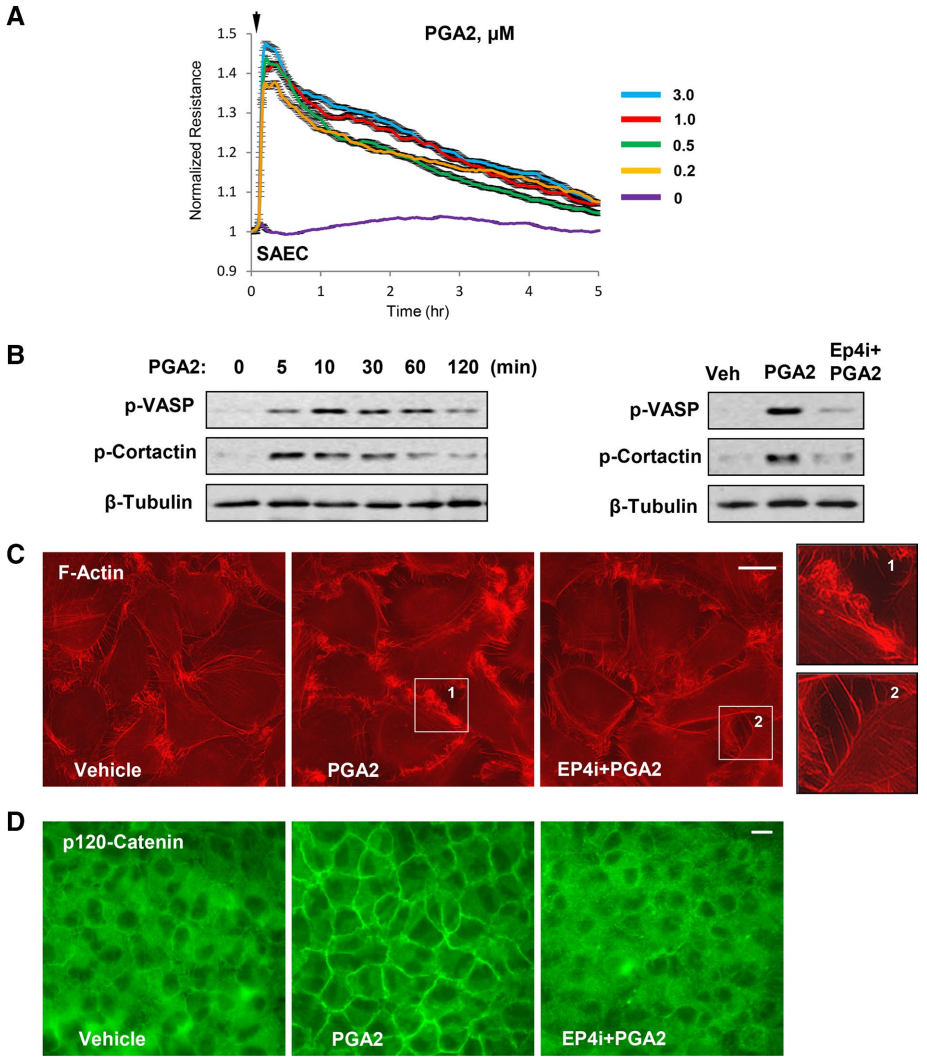

FIGURE 6: PGA2 effects on lung epithelial cell barrier, actin cytoskeleton, and cell junctions. (A) Human pulmonary SAEC monolayers were grown on gold microelectrodes. At the time point indicated by the arrow, cells were treated with 0.2, 0.5, 1.0, or 3.0 μM PGA2, followed by measurements of TER. (B) Time-dependent phosphorylation of VASP and cortactin was determined in the total lysates using phosphoprotein-specific antibodies (left). Effect of pretreatment with EP4 inhibitor on PGA2-induced phosphorylation of VASP and cortactin was evaluated by Western blot analysis with phosphospecific antibodies (right). Equal protein loadings were confirmed by membrane reprobing with β-tubulin antibody. (C, D) Effect of EP4 inhibitor on PGA2-induced cortical actin remodeling and enhancement of cell junctions. (C) Increased F-actin immunoreactivity in cell cortical area caused by PGA2 (0.5 μM, 5 min) was inhibited by pretreatment with EP4 inhibitor L161982. Higher-magnification insets depict details of cortical actin remodeling. Immunofluorescence staining was performed using Texas red–phalloidin. Bar, 5 μm. (D) SAEC monolayers grown on glass coverslips were stimulated with PGA2 (0.5 μM, 15 min) with or without pretreatment with EP4 inhibitor (L161982, 3 μM), followed by immunofluorescence staining for p120-cadherin. Bar, 10 μm. Results are representative of three independent experiments.

LPS. Two i.v. injections of PGA2, concurrently and 5 h after LPS instillation, significantly decreased BAL protein content and total cell count in the LPS-treated mice (Figure 11A). Effects of PGA2 on the lung vascular leak induced by LPS were further evaluated by measurement of Evans blue extravasation into the lungs. PGA2 treatment suppressed LPS-induced Evans blue accumulation in the lung parenchyma (Figure 11B).

Next, to evaluate the rate of ALI recovery, we performed image analysis of PGA2 effects on lung recovery after LPS-induced injury. Lung vascular leak in mice treated with LPS and PGA2 was monitored in the same animals prospectively 1, 2, 3, and 6 d after treatment. Lung accumulation of the Angiosense 680 EX tracer was performed in anesthetized animals using noninvasive fluorescence optical imaging as described in *Materials and Methods*. Accumulation of the fluorescent tracer reflecting lung inflammation and vascular barrier compromise increased 24 and 48 h after LPS injection and gradually declined by day 6 (Figure 11C). Of importance, LPS-induced lung dysfunction was markedly reduced by PGA2 treatment (two injections, concurrently and 5 h after LPS challenge), and recovery of lung function occurred earlier than in LPS-challenged mice without PGA2 treatment.

Protective effects of PGA2 in vivo are mediated by endothelial EP4

To test the role of endothelial EP4 in the mediation of the barrier-protective and anti-inflammatory effects of PGA2 in vivo, we used endothelial EP4-knockout mice generated by cross-breeding of the inducible endothelial VECad-Cre-ER^{T2} line (Monvoisin *et al.*, 2006) and EP4$^{lox/lox}$ mice. Generation and characterization of EC-specific EP4-knockout mice (*EC-EP4–/–*) were described previously (Liang *et al.*, 2011). First, we evaluated the magnitude of LPS-induced lung injury in *EC-EP4–/–* mice and matching controls. Parameters of lung injury were analyzed 24 h after LPS administration. *EC-EP4–/–* mice developed higher levels of lung injury in response to LPS, which was reflected by increased total and neutrophil cell counts and protein content in BAL samples (Figure 12A). Of greater importance, PGA2 treatment significantly attenuated parameters of LPS-induced lung injury and vascular leak in wild-type controls, as reflected by reduced cell count and protein content in BAL samples (Figure 12A) and decreased Evans blue accumulation in lung parenchyma (Figure 12B). In contrast, this lung-protective effect of PGA2 treatment was abolished in *EC-EP4–/–* mice. Western blot analysis of lung tissue samples also revealed increased ICAM1 expression in *EC-EP4–/–* mice and matching wild-type controls after 24 h of LPS challenge (Figure 12C). LPS-induced activation of ICAM1 expression was strongly suppressed by PGA2 treatment of wild-type mice but remained at levels similar to those for animals treated with LPS alone in *EC-EP4–/–* mice. Taken together, these results demonstrate pronounced anti-inflammatory and barrier-protective effects of PGA2 in the two animal models of ALI and emphasize a key role for endothelial EP4 receptor in PGA2-induced protection against LPS-induced lung vascular inflammation, barrier dysfunction, and lung injury.

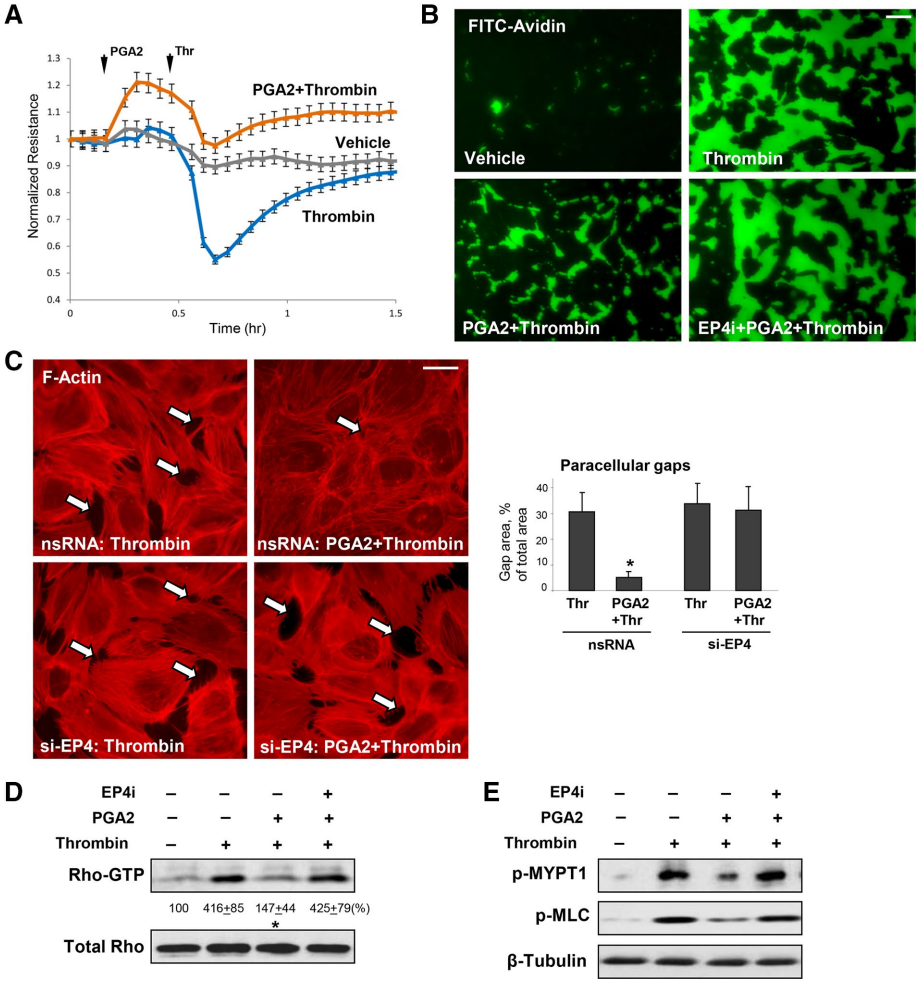

FIGURE 7: PGA2 attenuates thrombin-induced EC permeability in an EP4-dependent manner. (A) Pulmonary ECs plated on gold microelectrodes for TER measurements were treated with PGA2 (0.5 μM) at the time indicated by the first arrow, followed by thrombin (0.3 U/ml) stimulation as marked by the second arrow. Results are representative of five independent experiments. (B) Visualization of permeability in EC monolayers grown on biotinylated gelatin substrate and pretreated with vehicle or PGA2 followed by stimulation with thrombin in the presence of absence of EP4 inhibitor, using FITC-avidin as tracer, as described in *Materials and Methods*. Results are representative of four independent experiments. Bar, 20 μm. (C) Effect of PGA2 (0.3 μM, 10 min) on thrombin (0.5 U/ml, 15 min)–induced formation of actin stress fibers and paracellular gaps. The protective effect of PGA2 was abolished in ECs with siRNA-induced EP4 knockdown. Immunofluorescence staining was performed using Texas red–phalloidin. Paracellular gaps are marked by arrows. Results are representative of three independent experiments. Bar, 10 μm. Bar graph represents results of quantitative analysis of paracellular gap formation, shown as mean ± SD; $n = 3$; $^*p < 0.05$. (D) Thrombin-induced activation of RhoA measured in pull-down assays was suppressed by pretreatment with PGA2. EP4 inhibitor abolished the effects of PGA2. Results of densitometry are shown as mean ± SD; $n = 3$; $^*p < 0.05$. (E) Thrombin-induced phosphorylation of Rho kinase targets MYPT and MLC detected by Western blot was suppressed by pretreatment with PGA2. EP4 inhibitor abolished effects of PGA2. Membrane reprobing with antibody to β-tubulin was used as a normalization control.

DISCUSSION

The role of PGA2 in regulation of endothelial permeability and lung inflammatory response to bacterial pathogens remains virtually unknown. This is the first report demonstrating PGA2 vascular protective and anti-inflammatory effects in vitro and in vivo. PGA2 caused sustained barrier enhancement of pulmonary EC monolayers, dramatically attenuated EC permeability caused by thrombin, and restored the barrier function of EC monolayers challenged with LPS.

Cell membrane receptor(s) mediating PGA2 effects are not well defined. An earlier study suggested PGA2 interaction with two groups of cell membrane receptors—one stimulating phospholipase C and calcium entry and the other stimulating production of cAMP (Muallem *et al.*, 1989). Both receptor types were also activated by other PGs: PGE2, PGI2, PGF2α, and others. We screened potential receptors engaged in PGA2 signaling and identified EP4 as a receptor mediating vascular endothelial barrier–protective and anti-inflammatory effects of PGA2 in vitro and in vivo. This novel finding was further verified using a genetic model of EC-specific EP4-knockout mice. EP4 is a Gs-coupled receptor stimulating cAMP production primarily activated by PGE2 but may also ligate PGF2α and PGD2 at much higher concentrations (Leduc *et al.*, 2009). Of interest, accumulating evidence suggests considerable functional selectivity among the structurally related prostaglandins. PGE2 was the most selective in activating Gαs, whereas PGF2α and PGE1 were the most biased for activating Gαi1 and β-arrestin, respectively (Leduc *et al.*, 2009). Physiological effects of PGE2, PGF2α, and PGD2 are quite different because these prostaglandins also interact with their other cognate receptors (EP1-3, FP and DP, respectively) and stimulate additional functional responses mediated by Gs-, Gq-, and Gi-coupled signaling pathways (Breyer *et al.*, 2001; Bos *et al.*, 2004). Furthermore, depending on receptor subtype, cell population, and the context of activation, PGE2 displays pro- and anti-inflammatory effects, whereas PGI2 and its stable analogues have mostly anti-inflammatory and barrier-protective properties (Hata and Breyer, 2004; Birukova *et al.*, 2013b; Schlegel and Waschke, 2014). These unique patterns of receptor activation by each class of prostaglandin likely define the specific type of tissue or organ response to these mediators.

Ligation of EP4 receptor stimulates Gα-protein–mediated transient increase in intracellular cAMP (Sugimoto and Narumiya, 2007). In turn, cAMP activates PKA, which then phosphorylates downstream effector proteins—in particular, CREB. In addition, elevation of intracellular cAMP activates the PKA-induced independent pathway mediated by cAMP-stimulated guanine nucleotide exchange factor EPAC (Bos, 2006).

Activation of Rap1, Rac1, and PKA pathways observed in PGA2-stimulated EC is consistent with engagement of EP4 receptor and stimulation of downstream cell adhesion and cytoskeletal targets as a potential mechanism involved in the enhancement of the EC barrier. Activation of Rac1 by PGA2 in this study was accompanied by peripheral translocation of cortactin linked to EC barrier enhancement (Tian *et al.*, 2014). PKA-dependent phosphorylation of another

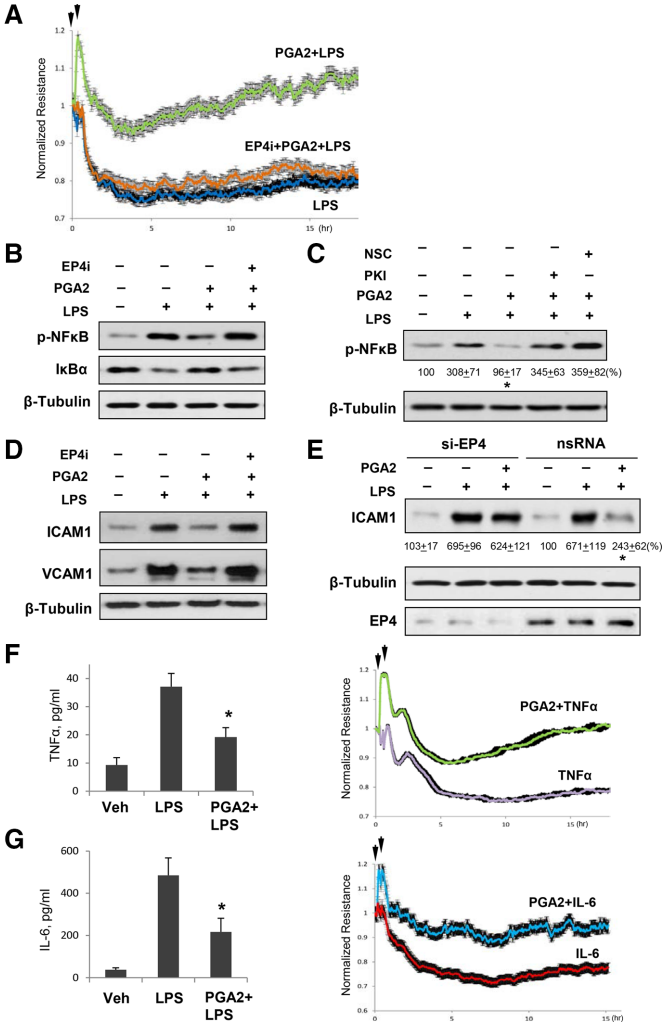

FIGURE 8: PGA2 attenuates LPS-induced EC barrier dysfunction and inflammatory activation in an EP4-dependent manner. (A) Pulmonary ECs were treated with PGA2 (first arrow) and stimulated with LPS (200 ng/ml, second arrow) with or without pretreatment with EP4 inhibitor. TER measurements were performed over a 18-h time period. (B) ECs were preincubated with vehicle or EP4 inhibitor (45 min) before PGA2 pretreatment (15 min), followed by LPS stimulation. NFκB phosphorylation and IκBα degradation were evaluated 1 h after LPS addition (left); ICAM1 and VCAM1 expression was evaluated 6 h after LPS addition (right). (C) Effect of pretreatment with Rac inhibitor (NSC, 100 μM, 30 min) and PKA inhibitor (PKI, 20 μM, 30 min) on PGA2-mediated inhibition of LPS-induced NFκB phosphorylation. Results of densitometry are shown as mean ± SD; $n = 4$; *$p < 0.05$. Effect of (D) EP4 inhibitor pretreatment (30 min) and (E) EP4 knockdown on PGA2-mediated inhibition of LPS-induced ICAM1 and VCAM1 expression. ECs were transfected with EP4-specific siRNA or nonspecific RNA 72 h before agonist stimulation. Reprobing with β-tubulin antibody was used as normalization control. Efficiency of EP4 knockdown was verified by Western blot. Results of densitometry are shown as mean ± SD; $n = 4$; *$p < 0.05$. LPS induces production of TNFα (F) and IL-6 (G) by pulmonary ECs (left), which contribute to pulmonary EC barrier dysfunction (right). PGA2 pretreatment attenuates both the LPS-induced TNFα and IL-6 production and the cytokine-induced EC permeability. Results shown as mean ± SD of three independent experiments; *$p < 0.001$. Addition of PGA2 and cytokines in TER experiments is marked by arrows.

actin-binding protein, VASP, which was observed in PGA2-stimulated ECs, leads to structural relaxation of the actin cytoskeleton, its linkage with tight junctions via the VASP/ZO-1 complex (Comerford *et al.*, 2002). PGA2 in this study increased association of VASP with the AJ protein α-catenin and other AJ–TJ complex members—p120-catenin, VE-cadherin, and ZO-1. This functional association reflects PGA2-induced enhancement of the EC barrier via increased interactions between AJ and TJ complexes assisted by VASP. In turn, pharmacological or molecular inhibition of EP4 receptor attenuated PGA2-induced activation of peripheral actin cytoskeleton, AJ and TJ assembly, and formation of the VASP/AJ/TJ functional complex. Whereas direct interaction of VASP and α-catenin at the AJs has been reported (Kobielak and Fuchs, 2004), the presence of VASP in ZO-1, p120-catenin, and VE-cadherin complexes may reflect functional AJ–TJ interactions contributing to PGA2/EP4-induced EC barrier enhancement.

Of interest, PGA2 also induced the barrier-enhancing response and remodeling of peripheral actin cytoskeleton and cell junctions in pulmonary epithelial cells; however these effects were less sustained. These results may indicate cell type–specific differences in PGA2 effects. In addition to pulmonary artery ECs, PGA2 also exhibited barrier protective effects in LPS-challenged lung microvascular EC monolayers (unpublished data). Such complementary PGA2 effects on both lung endothelial and epithelial cells may further promote lung barrier function in the ALI settings in vivo. However, in this study, we focused on the endothelial side, and the i.v. route of PGA2 administration used in this study more specifically targeted pulmonary endothelium.

PGA2 attenuated EC barrier dysfunction caused by thrombin. This effect is consistent with attenuation of thrombin-induced RhoA signaling, a major pathway of EC barrier dysfunction. Our result show that PGA2 induced activation of Rap1/Rac1/PKA signaling, which was previously shown to down-regulate barrier-disruptive RhoA signaling via mechanisms of negative cross-talk (Wildenberg *et al.*, 2006; Birukova *et al.*, 2013a).

Besides the canonical activation by the TLR4-MyD88-IRAK-TRAF6 cascade, LPS-induced stimulation of RhoA pathway also contributes to the activation of p38 mitogen-activated protein kinase (MAPK) and inflammatory response. Activated p38 MAPK phosphorylates the NFκB RelA/p65 subunit, which further stimulates NFκB transcription activity (Nwariaku *et al.*, 2003; Matoba *et al.*, 2010; Guo *et al.*, 2012b). Inhibition of Rho activities by *Clostridium difficile* toxin B, inhibition of RhoA nucleotide exchange factor GEF-H1, or p38 MAPK knockdown suppressed the LPS-induced NFκB phosphorylation and transactivation and increased IL-8 synthesis (Guo *et al.*, 2012a). Our data show that PGA2-induced elevation of cAMP was associated with activation of Rap1 and Rac1 GTPases (Figure 2). PGA2 pretreatment attenuated agonist-induced activation of RhoA (Figure 7) and inflammatory signaling, including LPS-induced NFκB phosphorylation (Figure 8). In turn, inhibition of Rac1 attenuated anti-inflammatory effects of PGA2 and restored the increased NFκB phosphorylation caused by LPS. These findings are in line with work showing that inhibition of Rho signaling by the activated Rap1/Rac1 cascade down-regulated the lung inflammation and barrier dysfunction in the model of ventilator-induced lung injury (Birukova *et al.*, 2012).

Our data also demonstrate an additional PKA-dependent mechanism of the cAMP anti-inflammatory effect. Inhibition of PKA blocked effects of PGA2 on LPS-induced phosphorylation of NFκB (Figure 8C). Increased intracellular cAMP in endothelial cells was

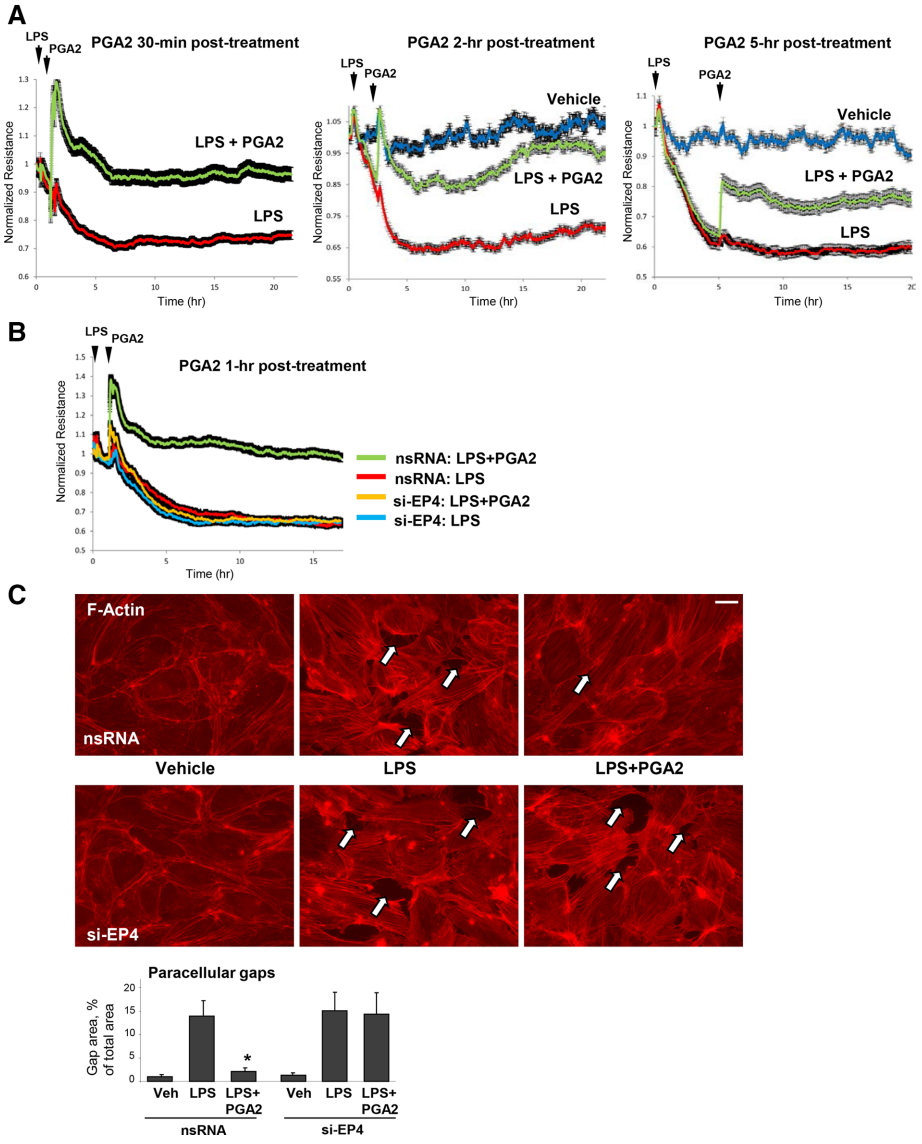

FIGURE 9: Posttreatment with PGA2 recovers LPS-induced EC permeability and monolayer disruption in an EP4-dependent manner. (A) Pulmonary ECs plated on microelectrodes were stimulated with LPS (200 ng/ml), followed by PGA2 (0.5 μM) posttreatment at different time points after LPS challenge, as shown by arrows. TER changes reflecting EC monolayer barrier properties were monitored over 20 h after treatments. (B) Pulmonary ECs transfected with nonspecific or EP4-specific siRNA 72 h before agonist stimulation were challenged with LPS (first arrow) and then treated with PGA2 (second arrow). TER measurements were performed over an 18-h time period. (C) ECs transfected with nonspecific or EP4-specific siRNA were challenged with LPS and treated 5 h later with PGA2 or vehicle. Analysis of actin cytoskeletal rearrangement 1 h after PGA2 posttreatment was performed by immunofluorescence staining with Texas red–phalloidin. Paracellular gaps are marked by arrows. Bar graph represents results of quantitative analysis of paracellular gap formation, shown as mean ± SD; $n = 4$; *$p < 0.05$. Bar, 10 μm.

previously found to prevent NFκB-dependent ICAM-1 expression induced by inflammatory agonists. Elevation of intracellular cAMP in pulmonary ECs blocked p38 MAPK activation in a PKA-dependent manner, which prevented NFκB RelA/p65 subunit phosphorylation and transcriptional activity of nuclear DNA-bound NFκB (Rahman *et al.*, 2004).

Previous work also shows the anti-inflammatory effects of PGA2 on other cells involved in the inflammatory response. PGA_2 inhibited the production of NO, IL-1β, TNF-α, IL-6, and MCP-1 from astrocytes stimulated with LPS (Storer *et al.*, 2005). Cyclopentenone isoprostanes also inhibited the inflammatory response in macrophages. PGA2 potently inhibited LPS-stimulated IκBα degradation and subsequent NFκB nuclear translocation and transcriptional activity in macrophages. PGA2-induced inhibition of the NFκB pathway in macrophages was at least partially mediated by a redox-dependent mechanism (Musiek *et al.*, 2005). However, evaluation of PGA2-EP4 mechanism of anti-inflammatory effects in other cells was beyond the scope of this study.

Of importance, PGA2 had potent protective effects in two animal models of ALI—one due to i.t. instillation of LPS and the other to mechanical ventilation at high tidal volume and injection of TRAP peptide. In both models, PGA2 treatment improved lung vascular endothelial barrier function, as indicated by decreased cell and protein content in BAL samples and decreased extravasation of Evans blue tracer into the lung parenchyma. These effects were also observed in the setting of more clinically relevant PGA2 posttreatment. Experiments with noninvasive optical imaging of LPS-challenged mice with or without PGA2 treatment made it possible to monitor the progression and recovery of ALI. The role of endothelial EP4 receptor in the barrier-protective and anti-inflammatory effects of PGA2 observed in animal models was confirmed in a genetic model of EC-specific ablation of EP4 receptor. In these experiments, conditional deletion of EP4 in vascular endothelium abolished the anti-inflammatory and barrier-protective effects of PGA2 treatment.

In summary, this study described PGA2-induced barrier-enhancing and barrier-protective effects in cell and animal models of endothelial vascular leak, inflammation, and lung barrier dysfunction. We identified EP4 as a receptor mediating barrier-protective and anti-inflammatory effects of PGA2 in pulmonary endothelium and described PGA2-induced cell junction and cytoskeletal remodeling contributions to protection of the lung endothelial barrier. Our results suggest that PGA2 may also enhance resolution of lung injury and accelerate EC barrier restoration.

MATERIALS AND METHODS

Cell culture and reagents

Human pulmonary artery endothelial cells, small airway epithelial cells (SAEC), and cell culture basal medium with growth supplements were obtained from Lonza (Allendale, NJ). Cells were cultured according to the manufacturer's protocol and used at passages 5–7. All reagents for immunofluorescence studies were purchased from Molecular Probes (Eugene, OR). PGA2, EP4 agonist CAY10580, and prostaglandin receptor inhibitors were obtained from Cayman (Ann Arbor, MI). The following receptor inhibitors were

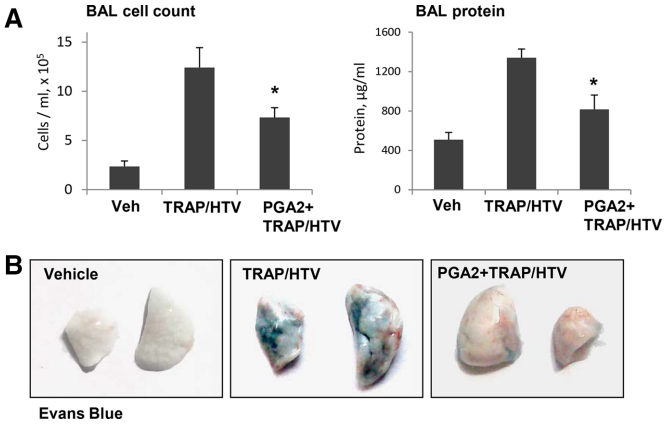

FIGURE 10: PGA2 attenuates HTV/TRAP6-induced lung injury and vascular leak. Mice were treated with PGA2 (10 µg/kg, i.v.) or vehicle twice, concurrently with TRAP6 injection (1.5×10^{-5} mol/kg, i.t.) followed by mechanical ventilation at high tidal volume (HTV, 30 ml/kg, 4 h). (A) Measurements of total cell count (left) and protein concentration (right) in BAL fluid; *$p < 0.05$; $n = 6$. (B) Vascular leak was analyzed by Evans blue–labeled albumin extravasation into the lung tissue, as described in *Materials and Methods*. Shown are representative images of lungs excised from the chest and perfused with PBS; $n = 4$.

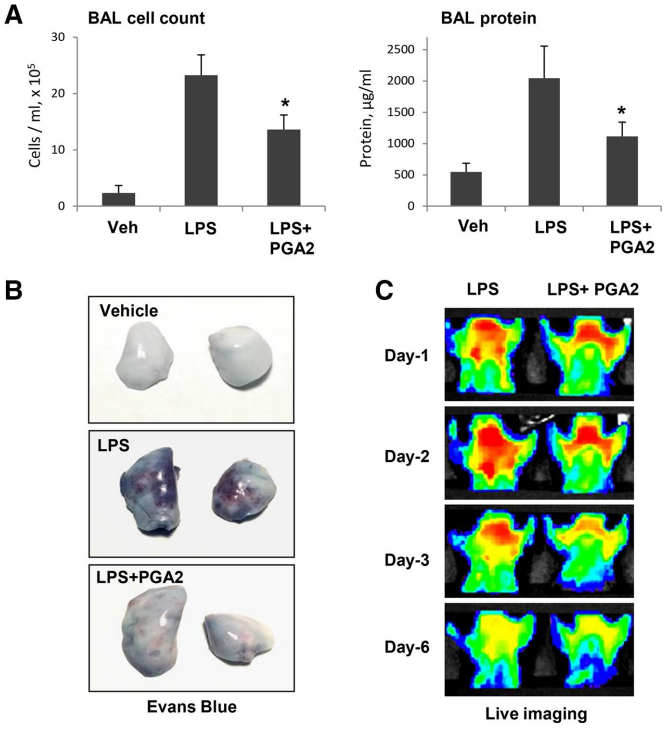

FIGURE 11: PGA2 attenuates LPS-induced lung injury and vascular leak. PGA2 was injected (i.v.) twice, concurrently and 5 h after i.t. LPS administration. The experiment was terminated after 24 h of LPS challenge. (A) Total cell count (left) and protein concentration (right) in BAL fluid; *$p < 0.05$; $n = 8$. (B) Vascular leak is reflected by Evans blue–labeled albumin extravasation into the lung tissue. Images of lungs excised from the chest and perfused with PBS. (C) Optical imaging of lung vascular barrier dysfunction after LPS challenge with and without PGA2 treatment. Accumulation of fluorescent Angiosense 680 EX imaging agent, reflecting lung vascular leak, was detected in lungs of the same animals by Xenogen IVIS 200 Spectrum imaging system at 1, 2, 3, and 6 d after LPS challenge; presented in arbitrary colors.

used: TP inhibitor SQ29548, DP inhibitor BWA868C, IP inhibitor CAY10449, EP4 inhibitors L161982 and GW627368X, FP inhibitor AL8810, and EP1-3 inhibitor AH6809. Rac1 inhibitor NAS23766 was obtained from EMD Millipore (Billerica, MA); PKA peptide inhibitor PKI was from Promega (Madison, WI). VE-cadherin antibody was obtained from Cayman; EP4, Rap1, Rac1, RhoA, ICAM1, and VCAM1 antibodies were obtained from Santa Cruz Biotechnology (Santa Cruz, CA); β-actin and β-tubulin antibodies were from Sigma-Aldrich (St. Louis, MO); cortactin, phospho-cortactin, VASP, phospho-VASP, phospho-CREB, phospho-MYPT, diphospho-MLC, phospho-NFκB, and IκBα antibodies were obtained from Cell Signaling (Beverly, MA); α-catenin, p120-catenin, and ZO-1 antibodies were from BD Transduction Laboratories (San Diego, CA). Unless specified, other biochemical reagents were obtained from Sigma-Aldrich.

Measurements of cAMP accumulation

Cells were seeded in 24-well culture plates. At the day of assay, the cells were stimulated with the PGA2 for desired periods of time. Cyclic AMP accumulation was quantified by cAMP Biotrak Enzyme Immunoassay (GE Healthcare Life Sciences, Pittsburgh, PA), and optical density was determined using a plate reader at 630 nm. Each sample/standard was analyzed in duplicate, and resulting OD values were averaged.

siRNA transfection

To reduce the content of endogenous EP4, cells were treated with gene-specific siRNA duplexes. A predesigned standard-purity, EP4-specific set of four siRNAs (*Homo sapiens*) was purchased from Dharmacon (Lafayette, CO), and transfection of ECs with 100 nM gene-specific siRNA or nonspecific, nontargeting siRNA (Dharmacon), which was used as a control treatment, was performed as previously described (Birukova *et al.*, 2007a). After 72 h of transfection, cells were used for experiments or harvested for Western blot verification of specific protein depletion. The siRNA transfection efficiency according to our protocol was >90% (Birukova *et al.*, 2007a).

Analysis of endothelial cell monolayer permeability

EC monolayer barrier properties were evaluated by two complementary methods. Analysis of agonist-induced changes in TER was performed using the ECIS Z electrical cell–substrate impedance-sensing system (Applied Biophysics, Troy, NY). This method allows measurements of TER in real time, which reflects agonist-induced EC permeability changes. Analysis of EC monolayer permeability for macromolecules was performed using Vascular Permeability Imaging Assay (17-10398; Millipore). The method is based on high-affinity binding of avidin-conjugated, FITC-labeled tracer added in cell culture medium during agonist stimulation to the biotinylated ligand in the substrate coating underlying EC monolayers. In permeability visualization experiments, cells grown on biotinylated gelatin–coated glass coverslips were fixed with 3.7% formaldehyde in PBS (10 min, room temperature), and imaging of areas with substrate-bound FITC-avidin was performed as described elsewhere (Birukova *et al.*, 2010).

Immunofluorescence and live-cell imaging

Endothelial cells plated on glass coverslips were treated with PGA2 with or without pretreatment with inhibitors, fixed in 3.7% formaldehyde in PBS for 10 min at 4°C, washed three times with PBS, permeabilized with 0.1% Triton X-100 in PBS-Tween (PBST) for 30 min at room temperature, and blocked with 2% bovine serum albumin (BSA) in PBST for 30 min. Incubations with antibodies of interest were performed in blocking solution (2% BSA in PBST) for 1 h at room

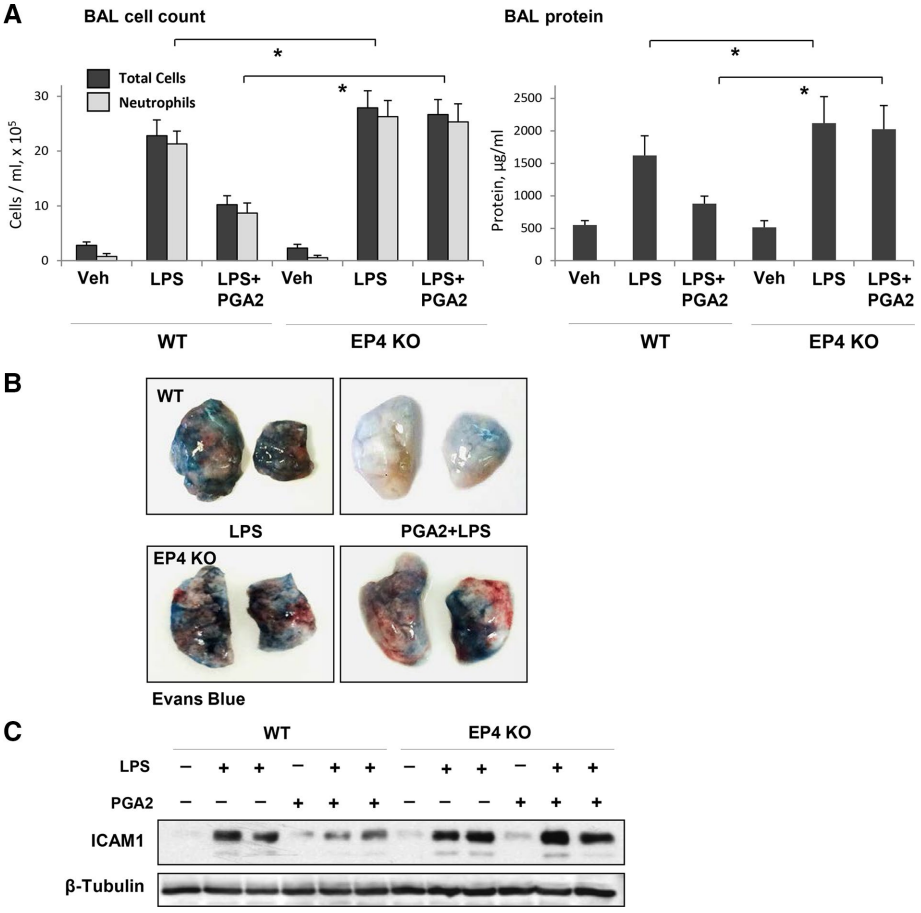

FIGURE 12: Endothelial-specific EP4 knockout increases LPS-induced lung barrier dysfunction and abolishes protective effects of PGA2 against LPS-induced lung injury. PGA2 injection (i.v.) of EC-specific *EP4+/+* and *EP–/–* mice was performed concurrently and 5 h after i.t. LPS administration. The experiment was terminated after 24 h of LPS challenge. (A) Total cell and neutrophil counts (right) and protein concentration (left) in BAL fluid; $*p < 0.05$; $n = 4$. (B) Vascular leak is reflected by Evans blue–labeled albumin extravasation into the lung tissue. Representative images of lungs excised from the chest and perfused with PBS; $n = 3$. (C) Protein expression of ICAM-1 in control and treated lung tissue samples evaluated by immunoblotting. Equal protein loading in Western blot experiments was confirmed by determination of β-tubulin content in tissue samples.

temperature, followed by staining with Alexa 488x or Alexa 544–conjugated secondary antibodies. Actin filaments were stained with Texas red–conjugated phalloidin. After immunostaining, slides were analyzed using a Nikon video imaging system (Nikon, Tokyo, Japan) as described elsewhere (Birukova *et al.*, 2004b). For live imaging of GFP-cortactin, cells were plated on MatTek dishes (MatTek, Ashland, MA) and transfected with GFP-cortactin plasmid (Addgene, Cambridge, MA). Time-lapse images were acquired with a 100×/numerical aperture (NA) 1.45 oil objective in a 3I Marianas Yokogawa-type spinning-disk confocal system equipped with a CO_2 chamber and a heated stage. Images were acquired with a 60×/NA 1.45 oil objective with 2-s intervals for 0.5–10 min. Quantitative analysis of paracellular gap formation, peripheral p120-catenin, ZO-1, and cortactin accumulation was performed as previously described (Birukova *et al.*, 2004a,c). For each experimental condition, at least 10 microscopic fields in each independent experiment were analyzed.

In situ proximal ligation assay

Cells were fixed with methanol/acetone and incubated for 30 min with the mouse anti–p120-catenin monoclonal antibody (BD Transduction Labs) and rabbit polyclonal anti-VE-cadherin antibody (Cayman). Ligation and amplification were performed as described in the manufacturer's protocol (Duolink In Situ PLA; Sigma-Aldrich), using the following reagents: PLA probe anti-rabbit plus; PLA probe anti-mouse minus, and detection reagent Red. After PLA, the samples were incubated for an additional 30 min with FITC-labeled donkey antibody against mouse immunoglobulin G.

Surface protein biotinylation

Cells were treated with 0.5 µM PGA2, washed with PBS at 37°C, and incubated for 10 min with 5 mM Sulfo-NHS-SS-Biotin (Pierce Biotechnology, Rockford, IL) at room temperature. Subsequently cells were washed two times with ice-cold PBS with 100 mM glycine and lysed for 30 min on ice in 1% Triton-100 PBS, and cell lysate was centrifuged at 10,000 × *g* for 10 min at 4°C. Equal amounts of cell lysate were incubated with 60 µl of streptavidin-agarose (Pierce Biotechnology, Rockford, IL) for 1 h at 4°C. Beads were washed three times with ice-cold PBS and boiled in SDS sample buffer with 5% 2-mercaptoethanol. Samples were centrifuged for 1 min at 1000 × *g*, and supernatants were subjected to Western blot analysis with VE-cadherin antibody.

Coimmunoprecipitation and immunoblotting

Protein extracts from cell or mouse lung tissue samples were separated by SDS–PAGE and transferred to polyvinylidene difluoride membranes, and the membranes were incubated with antibodies of interest. Equal protein loading was verified by probing of membranes with antibody to β-tubulin or a specific protein of interest. Coimmunoprecipitation studies were performed as described elsewhere (Birukova *et al.*, 2007b). Briefly, after agonist stimulation, plated EC cultures were washed in cold PBS and lysed on ice with cold TBS-NP40 lysis buffer (20 mM Tris, pH 7.4, 150 mM NaCl, 1% NP40) supplemented with protease and phosphatase inhibitor cocktails (Roche, Indianapolis, IN). Clarified lysates were then incubated with antibodies to VASP (Cell Signaling) or VE-cadherin (Cayman) overnight at 4°C and washed three or four times with TBS-NP40 lysis buffer, and the complexes were analyzed by Western blotting using appropriate antibodies. The relative intensities of the protein bands were quantified by scanning densitometry.

GTPase activation assays

Rac, Rap, and Rho activation was evaluated in pull-down assays using agarose beads with immobilized PAK1-PBD, Ral GDS-RBD, and rhotekin, respectively, as described elsewhere (Tian *et al.*, 2015). The levels of activated small GTPases bound to beads and evaluated by Western blot analysis were normalized to total Rac, Rap, and Rho levels.

Cytokine analysis

Concentrations of IL-6 and TNFα in control and treated cell-conditioned medium samples were measured using enzyme-linked immunosorbent assay kits from R&D Systems (Minneapolis, MN) according to manufacturer's instructions.

Animal studies

All experimental protocols involving the use of animals were approved by the University of Chicago Institutional Animal Care and Use Committee for the humane treatment of experimental animals. Endothelial-specific, EP4-knockout mice were previously described (Liang *et al.*, 2011). C57Bl6 mice were anesthetized with an intraperitoneal injection of ketamine (75 mg/kg) and acepromazine (1.5 mg/kg) and subjected to mechanical ventilation as previously described (Birukova *et al.*, 2010, 2011a). Briefly, tracheotomy was performed, and the trachea was cannulated with a 20-gauge, 1-inch catheter tied into place to prevent air leak. The animals were then placed on a mechanical ventilator (Harvard Apparatus, Boston, MA). Mice received PGA2 (10 μg/kg, i.v. administration) before a single dose of TRAP6 (1.5×10^{-5} mol/kg, i.t. instillation), followed by 4 h of mechanical ventilation with high tidal volume (30 ml/kg, 75 breaths/min, and 0 positive end expiratory pressure, HTV). Control animals were anesthetized and allowed to breathe spontaneously. In the model of LPS-induced lung injury, bacterial LPS (0.63 mg/kg body weight; *Escherichia coli* O55:B5) or sterile water was injected i.t. in a small volume (20–30 μl) using a 20-gauge catheter (Penn-Century, Philadelphia, PA). PGA2 (10 μg/kg) or sterile saline solution was administrated two times, concurrently and after 5 h of LPS instillation, by i.v. injection in the external jugular vein. Animals were killed by exsanguination under anesthesia 24 h after LPS challenge and used for evaluation of lung injury parameters.

Evaluation of lung injury parameters

After the experiment, collection of BAL fluid was performed using 1 ml of sterile Hanks balanced saline buffer. The BAL protein concentration was determined by a BCATM Protein Assay Kit (Thermo Scientific, Pittsburgh, PA). BAL inflammatory cell counting was performed using a standard hemacytometer technique (Fu *et al.*, 2009). Evans blue accumulation in the lung tissue was evaluated as described previously (Fu *et al.*, 2009). At the end of the experiment, thoracotomy was performed, and the lungs were perfused in situ via the left atrium with PBS containing 5 mM EDTA to flush the blood off the lungs. Left and right lungs were excised and imaged by a Kodak digital camera.

In vivo optical imaging

Mice treated with LPS or cotreated with PGA2 and LPS were injected i.v. via tail vein with 100 μl of 2 nmol Angiosense 680 EX (a vascular fluorescent blood pool imaging agent purchased from PerkinElmer, Boston, MA; NEV10054EX). After 24 h, fluorescence optical imaging was performed in the Integrated Small Animal Imaging Research Resource at the University of Chicago using the Xenogen IVIS 200 Spectrum (Caliper Life Sciences, Alameda, CA). Mice were exposed to isoflurane anesthesia with O_2 through the gas anesthesia manifold and placed on the imaging stage. Acquisition and image analysis were performed with Living Image 4.3.1 Software.

Statistical analysis

Results are expressed as means ± SD. Experimental samples were compared with controls by unpaired Student's *t* test. For multiple-group comparisons, a one-way analysis of variance and post hoc multiple comparison tests were used. $p < 0.05$ was considered statistically significant.

ACKNOWLEDGMENTS

This work was supported by Grants HL076259, HL087823, HL107920, and HL130431 from the National Heart, Lung, and Blood Institute and GM114171 from the National Institute of General Medical Sciences.

REFERENCES

Alfranca A, Iniguez MA, Fresno M, Redondo JM (2006). Prostanoid signal transduction and gene expression in the endothelium: role in cardiovascular diseases. Cardiovasc Res 70, 446–456.

Bazzoni G, Dejana E (2004). Endothelial cell-to-cell junctions: molecular organization and role in vascular homeostasis. Physiol Rev 84, 869–901.

Birukova AA, Alekseeva E, Mikaelyan A, Birukov KG (2007a). HGF attenuates thrombin-induced permeability in the human pulmonary endothelial cells by Tiam1-mediated activation of the Rac pathway and by Tiam1/Rac-dependent inhibition of the Rho pathway. FASEB J 21, 2776–2786.

Birukova AA, Birukov KG, Smurova K, Adyshev DM, Kaibuchi K, Alieva I, Garcia JG, Verin AD (2004a). Novel role of microtubules in thrombin-induced endothelial barrier dysfunction. FASEB J 18, 1879–1890.

Birukova AA, Fu P, Wu T, Dubrovskyi O, Sarich N, Poroyko V, Birukov KG (2012). Afadin controls p120-catenin-ZO-1 interactions leading to endothelial barrier enhancement by oxidized phospholipids. J Cell Physiol 227, 1883–1890.

Birukova AA, Fu P, Xing J, Yakubov B, Cokic I, Birukov KG (2010). Mechanotransduction by GEF-H1 as a novel mechanism of ventilator-induced vascular endothelial permeability. Am J Physiol Lung Cell Mol Physiol 298, L837–L848.

Birukova AA, Malyukova I, Poroyko V, Birukov KG (2007b). Paxillin-beta-catenin interactions are involved in Rac/Cdc42-mediated endothelial barrier-protective response to oxidized phospholipids. Am J Physiol Lung Cell Mol Physiol 293, L199–L211.

Birukova AA, Smurova K, Birukov KG, Kaibuchi K, Garcia JGN, Verin AD (2004b). Role of Rho GTPases in thrombin-induced lung vascular endothelial cells barrier dysfunction. Microvasc Res 67, 64–77.

Birukova AA, Smurova K, Birukov KG, Usatyuk P, Liu F, Kaibuchi K, Ricks-Cord A, Natarajan V, Alieva I, Garcia JG, Verin AD (2004c). Microtubule disassembly induces cytoskeletal remodeling and lung vascular barrier dysfunction: role of Rho-dependent mechanisms. J Cell Physiol 201, 55–70.

Birukova AA, Tian X, Tian Y, Higginbotham K, Birukov KG (2013a). Rap-afadin axis in control of Rho signaling and endothelial barrier recovery. Mol Biol Cell 24, 2678–2688.

Birukova AA, Wu T, Tian Y, Meliton A, Sarich N, Tian X, Leff A, Birukov KG (2013b). Iloprost improves endothelial barrier function in lipopolysaccharide-induced lung injury. Eur Respir J 41, 165–176.

Birukova AA, Zebda N, Cokic I, Fu P, Wu T, Dubrovskyi O, Birukov KG (2011a). p190RhoGAP mediates protective effects of oxidized phospholipids in the models of ventilator-induced lung injury. Exp Cell Res 317, 859–872.

Birukova AA, Zebda N, Fu P, Poroyko V, Cokic I, Birukov KG (2011b). Association between adherens junctions and tight junctions via Rap1 promotes barrier protective effects of oxidized phospholipids. J Cell Physiol 226, 2052–2062.

Bos CL, Richel DJ, Ritsema T, Peppelenbosch MP, Versteeg HH (2004). Prostanoids and prostanoid receptors in signal transduction. Int J Biochem Cell Biol 36, 1187–1205.

Bos JL (2006). Epac proteins: multi-purpose cAMP targets. Trends Biochem Sci 31, 680–686.

Breyer RM, Bagdassarian CK, Myers SA, Breyer MD (2001). Prostanoid receptors: subtypes and signaling. Annu Rev Pharmacol Toxicol 41, 661–690.

Comerford KM, Lawrence DW, Synnestvedt K, Levi BP, Colgan SP (2002). Role of vasodilator-stimulated phosphoprotein in PKA-induced changes in endothelial junctional permeability. FASEB J 16, 583–585.

Dubrovskyi O, Birukova AA, Birukov KG (2013). Measurement of local permeability at subcellular level in cell models of agonist- and ventilator-induced lung injury. Lab Invest 93, 254–263.

Fu P, Birukova AA, Xing J, Sammani S, Murley JS, Garcia JG, Grdina DJ, Birukov KG (2009). Amifostine reduces lung vascular permeability via suppression of inflammatory signalling. Eur Respir J 33, 612–624.

Fukata M, Kaibuchi K (2001). Rho-family GTPases in cadherin-mediated cell-cell adhesion. Nat Rev Mol Cell Biol 2, 887–897.

Guo F, Tang J, Zhou Z, Dou Y, Van Lonkhuyzen D, Gao C, Huan J (2012a). GEF-H1-RhoA signaling pathway mediates LPS-induced NF-kappaB transactivation and IL-8 synthesis in endothelial cells. Mol Immunol 50, 98–107.

Guo F, Zhou Z, Dou Y, Tang J, Gao C, Huan J (2012b). GEF-H1/RhoA signalling pathway mediates lipopolysaccharide-induced intercellular adhesion molecular-1 expression in endothelial cells via activation of p38 and NF-kappaB. Cytokine 57, 417–428.

Hata AN, Breyer RM (2004). Pharmacology and signaling of prostaglandin receptors: multiple roles in inflammation and immune modulation. Pharmacol Ther 103, 147–166.

Head JA, Jiang D, Li M, Zorn LJ, Schaefer EM, Parsons JT, Weed SA (2003). Cortactin tyrosine phosphorylation requires Rac1 activity and association with the cortical actin cytoskeleton. Mol Biol Cell 14, 3216–3229.

Howard LS, Morrell NW (2005). New therapeutic agents for pulmonary vascular disease. Paediatr Respir Rev 6, 285–291.

Khakpour S, Wilhelmsen K, Hellman J (2015). Vascular endothelial cell Toll-like receptor pathways in sepsis. Innate Immunity 21, 827–846.

Kobielak A, Fuchs E (2004). Alpha-catenin: at the junction of intercellular adhesion and actin dynamics. Nat Rev Mol Cell Biol 5, 614–625.

Leduc M, Breton B, Gales C, Le Gouill C, Bouvier M, Chemtob S, Heveker N (2009). Functional selectivity of natural and synthetic prostaglandin EP4 receptor ligands. J Pharmacol Exp Ther 331, 297–307.

Liang X, Lin L, Woodling NS, Wang Q, Anacker C, Pan T, Merchant M, Andreasson K (2011). Signaling via the prostaglandin E(2) receptor EP4 exerts neuronal and vascular protection in a mouse model of cerebral ischemia. J Clin Invest 121, 4362–4371.

Lu YC, Yeh WC, Ohashi PS (2008). LPS/TLR4 signal transduction pathway. Cytokine 42, 145–151.

Matoba K, Kawanami D, Ishizawa S, Kanazawa Y, Yokota T, Utsunomiya K (2010). Rho-kinase mediates TNF-alpha-induced MCP-1 expression via p38 MAPK signaling pathway in mesangial cells. Biochem Biophys Res Commun 402, 725–730.

Miyoshi J, Takai Y (2005). Molecular perspective on tight-junction assembly and epithelial polarity. Adv Drug Deliv Rev 57, 815–855.

Monvoisin A, Alva JA, Hofmann JJ, Zovein AC, Lane TF, Iruela-Arispe ML (2006). VE-cadherin-CreERT2 transgenic mouse: a model for inducible recombination in the endothelium. Dev Dyn 235, 3413–3422.

Muallem S, Merritt BS, Green J, Kleeman CR, Yamaguchi DT (1989). Classification of prostaglandin receptors based on coupling to signal transduction systems. Biochem J 263, 769–774.

Musiek ES, Gao L, Milne GL, Han W, Everhart MB, Wang D, Backlund MG, DuBois RN, Zanoni G, Vidari G, *et al*. (2005). Cyclopentenone isoprostanes inhibit the inflammatory response in macrophages. J Biol Chem 280, 35562–35570.

Nwariaku FE, Rothenbach P, Liu Z, Zhu X, Turnage RH, Terada LS (2003). Rho inhibition decreases TNF-induced endothelial MAPK activation and monolayer permeability. J Appl Physiol 95, 1889–1895.

Rahman A, Anwar KN, Minhajuddin M, Bijli KM, Javaid K, True AL, Malik AB (2004). cAMP targeting of p38 MAP kinase inhibits thrombin-induced NF-kappaB activation and ICAM-1 expression in endothelial cells. Am J Physiol Lung Cell Mol Physiol 287, L1017–L1024.

Schlegel N, Baumer Y, Drenckhahn D, Waschke J (2009). Lipopolysaccharide-induced endothelial barrier breakdown is cyclic adenosine monophosphate dependent in vivo and in vitro. Crit Care Med 37, 1735–1743.

Schlegel N, Waschke J (2014). cAMP with other signaling cues converges on Rac1 to stabilize the endothelial barrier—a signaling pathway compromised in inflammation. Cell Tissue Res 355, 587–596.

Smith CW (1993). Leukocyte-endothelial cell interactions. Semin Hematol 30, 45–53, discussion, 54–45.

Spindler V, Schlegel N, Waschke J (2010). Role of GTPases in control of microvascular permeability. Cardiovasc Res 87, 243–253.

Storer PD, Xu J, Chavis JA, Drew PD (2005). Cyclopentenone prostaglandins PGA2 and 15-deoxy-delta12,14 PGJ2 suppress activation of murine microglia and astrocytes: implications for multiple sclerosis. J Neurosci Res 80, 66–74.

Sugimoto Y, Narumiya S (2007). Prostaglandin E receptors. J Biol Chem 282, 11613–11617.

Tian Y, Gawlak G, Shah AS, Higginbotham K, Tian X, Kawasaki Y, Akiyama T, Sacks DB, Birukova AA (2015). Hepatocyte growth factor-induced Asef-IQGAP1 complex controls cytoskeletal remodeling and endothelial barrier. J Biol Chem 290, 4097–4109.

Tian Y, Tian X, Gawlak G, O'Donnell JJ 3rd, Sacks DB, Birukova AA (2014). IQGAP1 regulates endothelial barrier function via EB1-cortactin crosstalk. Mol Cell Biol 34, 3546–3558.

Wildenberg GA, Dohn MR, Carnahan RH, Davis MA, Lobdell NA, Settleman J, Reynolds AB (2006). p120-catenin and p190RhoGAP regulate cell-cell adhesion by coordinating antagonism between Rac and Rho. Cell 127, 1027–1039.

Yagami T, Koma H, Yamamoto Y (2016). Pathophysiological roles of cyclooxygenases and prostaglandins in the central nervous system. Mol Neurobiol 53, 4754–4771.